Geophysical Investigations on Gravity Gradiometry and Magnetic Data over the Wichita Uplift Region, Southwestern Oklahoma

by

Kamil Erkan

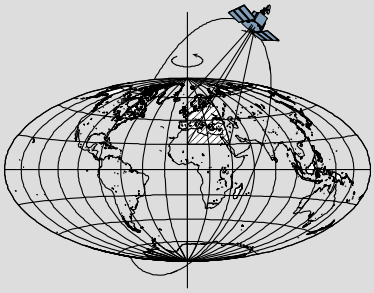

Report No. 509

Geodetic Science

The Ohio State University
Columbus, Ohio 43210

April 2015

Geophysical Investigations on Gravity Gradiometry and Magnetic Data over the Wichita Uplift Region, Southwestern Oklahoma

by

Kamil Erkan

Report No. 509

Geodetic Science

The Ohio State University
Columbus, Ohio

April 2015

PREFACE

This report was prepared by Dr. Kamil Erkan for work completed while on a post-doctoral fellowship at the School of Earth Sciences, Ohio State University, with support from research funds in the Geodetic Science Program. Dr. Erkan is now Professor in the Department of Civil Engineering, Marmara University, Goztepe, Istanbul, Turkey (E-mail: kamil.erkan@marmara.edu.tr).

ABSTRACT

The Wichita uplift in southwestern Oklahoma is a unique region that shows strong gravity and magnetic field anomalies. Detailed geologic data as well as structural cross sections are also available for the region. This report includes a qualitative geophysical analysis of the airborne gravity gradiometer profiles, and a quantitative analysis of an airborne magnetic field data collected in the region. Two datasets were analyzed independently. Firstly, an effort has been made by comparative analyses of different gravity gradient components with the gravity field from EGM2008 side by side in order to understand the nature of the subsurface structural setting. Secondly, a spectral analysis of magnetic field has been applied using the well-known power-law behavior of the magnetic field. The resulting source intensity map delineates the areas with high magnetic sources, and also is in agreement with the geologic findings in the region.

1. Introduction

The Wichita uplift in the southwestern Oklahoma is a unique region in terms of its geologic and tectonic setting. An extensive amount of data are available on the petrologic properties of the lithologic and structural units which shed light on its unique tectonic history (Keller and Baldridge, 1995). Adjacent to the uplifted area is the deepest continental basin of North America (Anadarko basin) with large amounts of hydrocarbon deposits (Perry, 1989). The general area is also unique by strong gravity and magnetic anomalies associated with the structural properties, and that is the main focus of this study.

In 1987, the first field test of Gravity Gradiometer Survey System (GGSS) was flown over a large of area of Texas/Oklahoma border including the Wichita uplift (Jekeli, 1988). The survey was the first field experience of the airborne gradiometry method. Quality of the data was studied by Brzezowski et al. (1988) and Jekeli (1993). An airborne magnetic survey by USGS is also available over the Wichita Mountains area, and also covers part of the GGSS survey area.

Geophysical interpretations have been made of the gravity gradient and the aeromagnetic field data. Vasco and Taylor (1991) mapped the basement topography of the uplifted region using GGSS data. Jekeli et al. (2010) compared the GGSS and the airborne magnetic data and showed that the Poisson's relation holds for the subsurface anomalies.

2. Geologic and Tectonic Setting

The Wichita Province consists of an uplifted basement unit between two deep basins, the Anadarko Basin in the north, and the Hollis basin in the south (Fig. 1). It is bounded in the north and south by a series of deep-incising fault zones. The eastern boundary of the uplifted area is more transitional with a thickening sedimentary layer toward the Ardmore Basin (Fig. 1). The western boundary of the uplifted area extends to the Texas pan-handle (not covered in Fig.1) changing its name to the Amarillo uplift. The Wichita section of the uplift zone shows the most profound structural and tectonic features while these features die away toward the Amarillo section.

The first and probably the most comprehensive geologic study on the general area including the uplifted section as well as the surrounding basins was made by Ham et al. (1964). This study includes dating the major rock units, generating structural cross sections based on data from 178 boreholes, analyzing petrochemical properties of the rock units, and finally making reconstructions for the structural evolution of the region (see, Fig. 2).

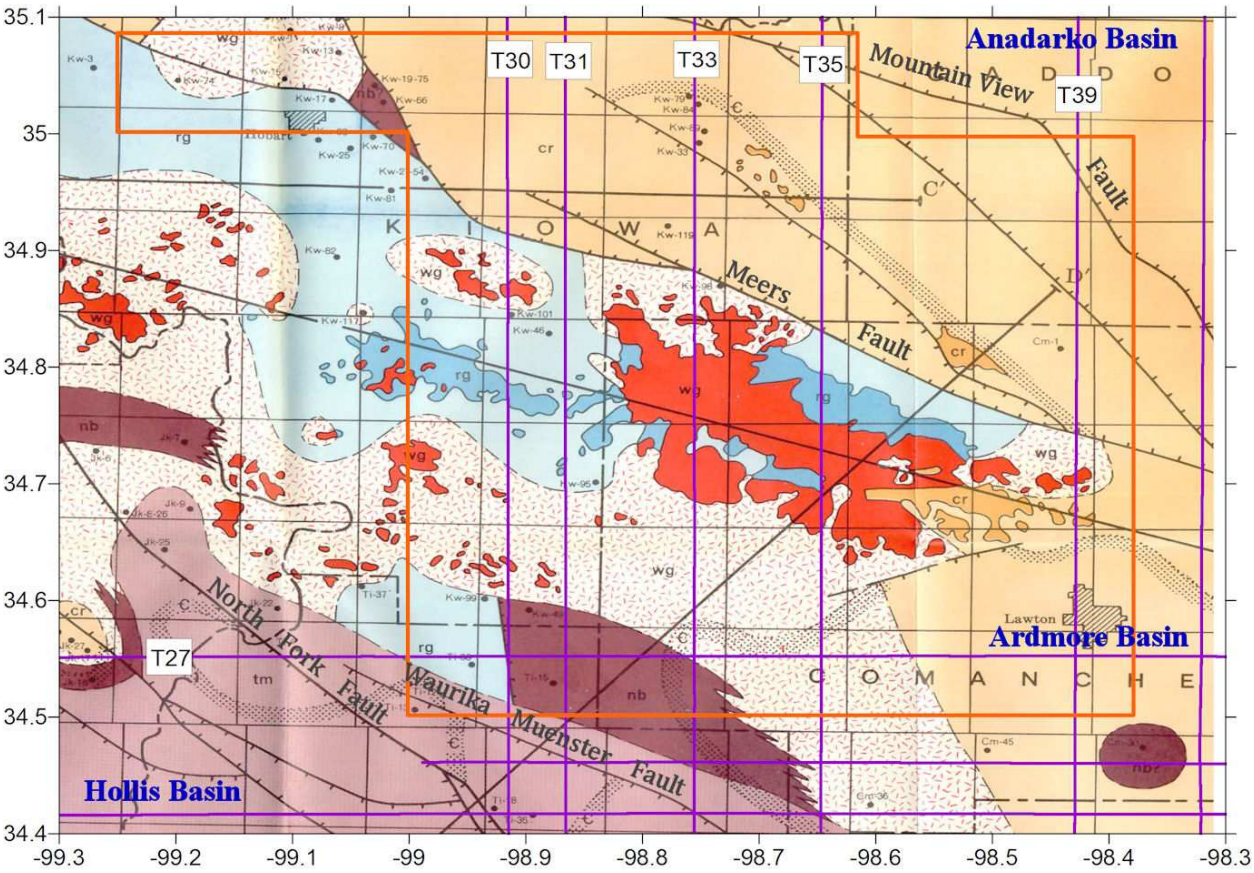

Figure 1: Basement geology of the Wichita uplift region (from Ham et al., 1964). Names of the units (also listed in Table 1) are as follows: wg: Wichita granite, cr: Carlton rhyolite, rg: Raggedy Mountain Gabbro group, nb: Navajoe basalt-spilite group, tm: Tillman metasedimentary unit. Red, dark blue, and orange color areas represent the outcropped part of the of the granite, rhyolite, and gabbro units. Major faults and surrounding basins are also shown. Purple colored lines show GGSS tracks; orange color lines show the boundary of the 1954 aeromagnetic survey.

The tectonic setting of the area was later described from the perspective of plate tectonics by Hoffman et al. (1974). They explained the area as an ideal example of an “aulacogen” (abandoned rift) rather than a “geosyncline” as described by Ham et al. (1964). Hoffman et al. (1974) also give examples of similar tectonic features in other parts of the world. Aulacogens form in the transverse direction to the general strike of rift zones but are located within the continental plate. During rifting, the aulacogen experiences bimodal (both silisic and basaltic) igneous activity. When the thermal pulse causing the igneous activity ceases, the crust starts to cool off, and shrinks vertically by thermal contraction which causes the formation of very deep basins around the rifted zone. Finally, due to their proximity to edges of the continental margins, a late stage contraction and uplift event occurs in these zones.

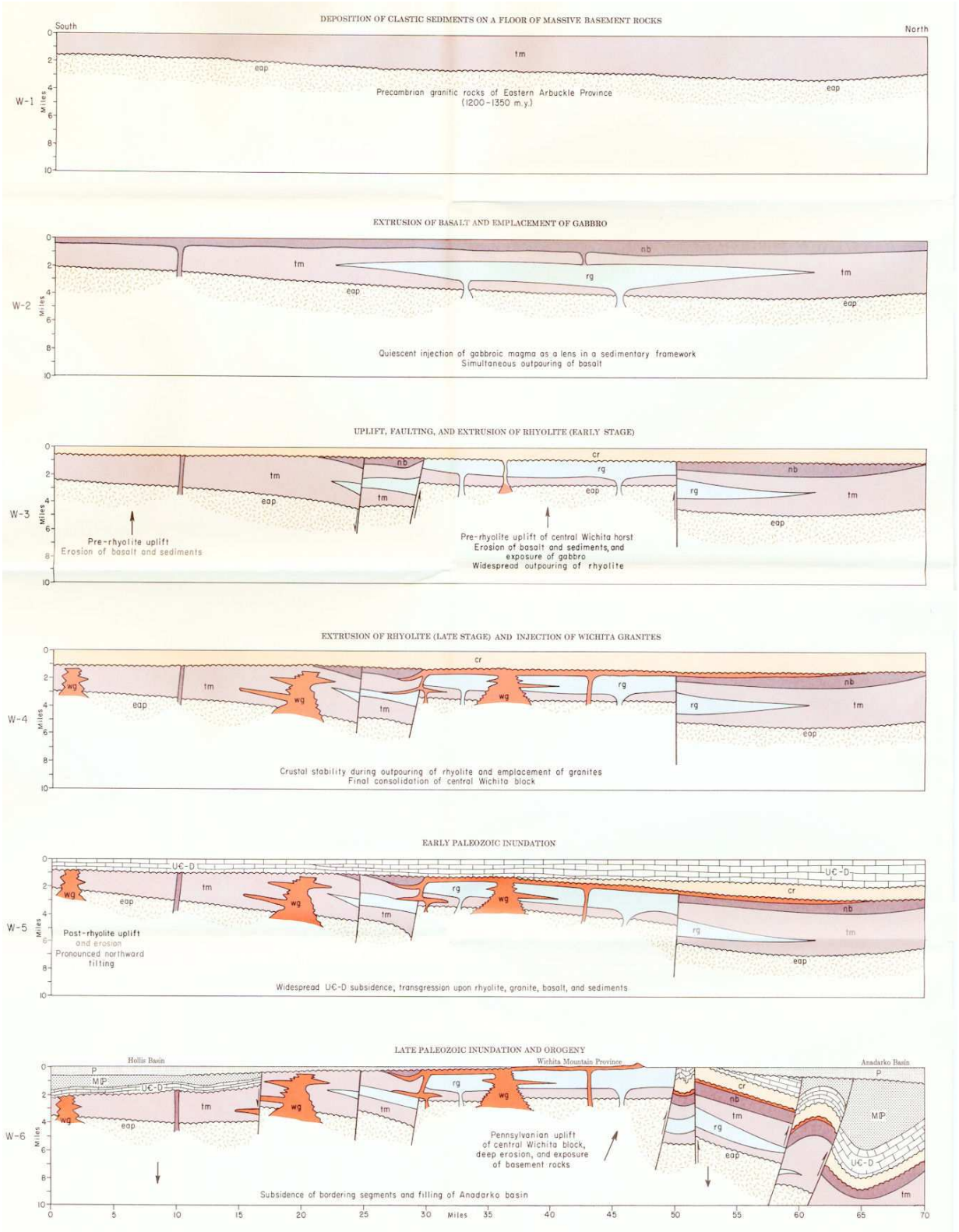

Figure 2: The major phases of the structural evolution of the study region (from Ham et al., 1964).

The structural evolution of the region can be divided into three episodes all of which occurred in the Paleozoic age (Ham et al., 1964; Fig. 2). The first period is the Early- to Mid-Paleozoic igneous activity associated with rifting of the continent. This magmatic/volcanic activity resulted in the formation of basement units of the Wichita province that we observe today. The multiple episodes of rifting also include the formation of high angle normal faults that are still present on both sides of the uplifted area. The second episode is the subsidence (sagging) of a large area encompassing the rifted area of Wichita province as a result of lithospheric cooling and thermal contraction. During this period, the subsided regions attracted large volumes of sediments during the Late Cambrian and Devonian periods. The third episode is the late Paleozoic orogeny and compression of the region. This compression led to re-activation of the boundary normal faults which turned to high-angle thrust faults. As an asymmetric basin, the Anadarko basin has formed during this period as a result of more than 2 km relative motion with respect to the Wichita region (Perry, 1989). The likely amount of vertical throw at the location of the Meers fault, which is the location of maximum uplift, exceeds 6.4 km (4 miles) during this stage. The uplift of the Wichita province at this stage was followed by exposure of the basement granite and gabbro units.

3. Major Petrologic Units

All structural features and associated rock units representing the uplifted area are Paleozoic in age (543-248 Ma) (Ham et al., 1964). There are five different types of basement rocks in the Wichita province (Table 1) excluding the older Precambrian rhyolite/granite basement which is part of the North America craton. Two of the units (Navajoe basalt-spilite and Tillman metasedimentary units) do not have surface exposures although they must cover a fairly substantial area under the surface (Fig. 1).

The oldest unit (Early Cambrian) is the Tillman metasedimentary group which underlies the Hollis basin and a small part of the uplifted area (Fig. 1). It has a thickness of ~5000 m under the basin. Its origin is before the magmatic/volcanic activity forming the Wichita uplift. The oldest units related to magmatic/volcanic activity in the region are the Raggedy Mountain gabbro group and the Navajoe basalt-spilite group which are both early Cambrian (~535 Ma) in age. These two units have the same chemical composition, implying that the second is the extrusive equivalent of the first. Navajoe basalt is found in a limited area south of the uplifted area and only encountered in drill cores (thickness of 300-1000 m). The gabbro unit covers the largest part of the Wichita uplift although only a small portion of it is exposed at the surface. It has an average thickness of 3000 m. The youngest igneous rocks in the Wichita province are the Carlton rhyolite group and Wichita granite group of middle Cambrian age (525-500 Ma). They have very similar chemical composition indicating that they are extrusive/intrusive equivalents of each other. Compared to the gabbro unit, the granite/rhyolite unit has a small thickness (~300 m), and is emplaced on the gabbro unit in the form of sills.

Table 1: Main basement units in the Wichita uplift area and some of their properties

Group name[1]	**Age**[1] **(Ma)**	**Av. Thickness**[1] **(m)**	**Av. Density**[2] **(g/cm^3)**	**Av. Susceptibility**[3] **(SI)**
Carlton rhyolite	525	200-500	2.65	$2x10^{-3}$
Wichita granite	525	200-500	2.65	$2x10^{-3}$
Navajoe basalt-spilite	535	300-1000	2.8	$5x10^{-2}$
Raggedy Mountain gabbro	535-570	3000	2.7-3.2	$3x10^{-2}$
Tillman meta-sedimentary unit	1000 (?)	5000	2.8	?
Rhyolite/granite terrane	1350-1400	-	2.67	?

[1]: Ham et al. (1964); Lambert et al. (1988); [2]: Coffman et al. (1986); Robbins and Keller (1992); [3]: Jones-Cecil (1995b); Price et al. (1998)

A northeast to southwest profile crossing the central Wichita uplift (Line D', see Fig.1) is shown in Fig. 3 (Ham et al., 1964). The profile outlines the horizontal and vertical extents of the basement units and their respective positions clearly.

Based on the stratigraphic units of the uplifted area and the basement structures of the surrounding basins, Ham et al. (1964) inferred two major episodes of uplift/erosion in the Wichita uplift. An earlier uplift occurred in ~535 Ma which resulted in the erosion of the Navajoe basalt intrusion of the rhyolite/granite units. A second episode of the uplift/erosion resulted in the removal of almost the entire rhyolite and overlying Devonian (370-350 Ma) sediments of the Wichita province. It is considered that the thickness of the rhyolite body was 1700-2300 m before the erosion episode as this area was the center of the igneous activity (Ham et al., 1964). The removal of the rhyolites/granite layers resulted in the exposure of the underlying gabbroic basement at the surface.

The basement largely exposes to the surface at the northern parts of the uplifted region (as mostly granites, see Fig.1, red colored units). Outside of the exposed areas the basement rocks are covered by a thin layer (< 300 m) of sedimentary rocks of Permian age (see Fig. 2, denoted by symbol P). The sedimentary layer has great thickness in the surrounding basins, and is the youngest unit of the Wichita province.

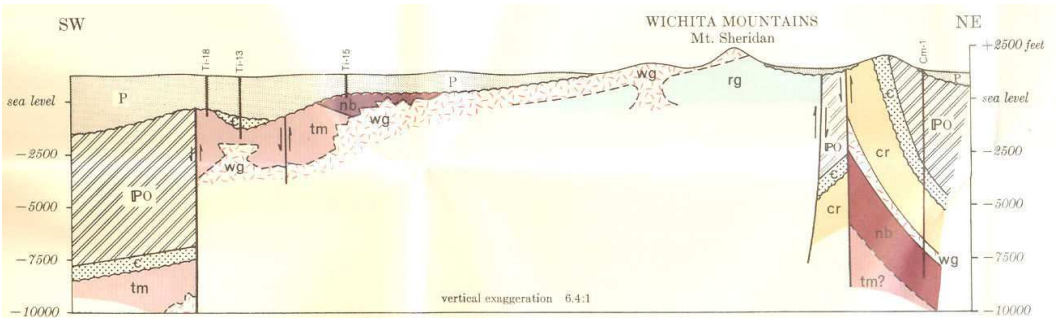

Figure 3: Cross section (Line D' in Fig. 1) showing the basement units in the Wichita uplift (from Ham et al., 1964).

In summary, the area of our interest, the Wichita province (Fig. 1), is bounded by two major fault zones in the north and south (Fig. 2) and is almost entirely composed of granite and gabbro units. The basalt and rhyolite units cover a very limited area within the Wichita uplift. Although the gabbro possesses a very large volume below the surface its surface exposure is limited due to emplacement of granitic units above it. Below the granite/gabbro basement units, 1.3-1.4 Gy old granite-rhyolite terrane is located (Table 1).

4. Previous Gravity and Magnetic Studies

Gravity measurements have been made at different times by different agencies. A local compilation of gravity data was made by Robbins and Baldridge (1995) using more than 11,000 points covering the uplifted area as well as the surrounding basins. They generated a residual isostatic gravity map with the actual data locations shown. In their map, as well as in the earlier gravity maps of the region, the entire uplifted area clearly shows up as an 80 mGal elongated positive gravity anomaly. The gravity anomaly here is the second largest one in amplitude after the mid-continental rift in the North American continent. The gravity anomaly cannot be explained by any changes in crustal thickness, and is entirely due to density variations within the upper crust. The sharp drops in the gravity field on both sides of the uplifted area indicate existence of large structural offsets.

Because of the elongated nature of the gravity signature, various 2D structural models were generated across the strike of the anomaly. Earlier studies pointed out a large mafic intrusion under the Wichita uplift to explain the observed gravity anomaly (Pruatt, 1974; Papesh, 1983). A more detailed structural model was made by Coffman et al. (1986) by including the petrologic and geologic constraints. According to this, the gravity high in the Wichita province is caused by two mafic intrusions, one that is shallow and the other is deep. The shallow one is located from the surface down to 3 km; whereas the deep mafic intrusion is located at 15-20 km in the upper

crust. The deep unit has slightly higher density than the shallow one. The deep unit is located inside the 1.3-1.4 Ga granite/rhyolite basement of the North American craton.

An alternative structural model assumes a single continuous mafic (gabbro) intrusion from the surface down to 20 km depth (Hamilton 1989; Robbins and Keller, 1992; Keller and Baldridge, 1995). In this model, the density of the mafic body increases with depth from 2.64 to 2.96 g/cm^3. In all of these models the common result is the existence of a deep mafic intrusion (continuous or discontinuous) from the surface down to as deep as 15-20 km.

The area of the interest was investigated by an aeromagnetic survey in 1954 by USGS (area bounded by the orange lines in Fig. 1), and data were published as a map (USGS, 1975). The survey altitude was 152 m with line spacing of 400 m along the E-W direction. In later years, this map was digitized and certain derivatives of the total field (e.g., reduction to the pole, RTP) were also published (Jones-Cecil, 1995a).

Earlier interpretations of the aeromagnetic data focused on the local change in the magnetic fields across the Meers fault (USGS, 1975). A similar study in later years also included a ground magnetic survey across the Meers fault, and more detailed models of the structural changes across the Meers fault were produced (Jones-Cecil, 1995b). A model of the Holocene reactivation of the Meers fault was also proposed. Jones-Cecil (1995b) also reports a collective summary of susceptibility measurements in the region. Other faults in the survey area were also delineated by combining the structural information with the magnetic field data. Another local study was done for one of the exposed gabbro-granite contacts south of the Wichita Mountains (Price et al., 1998).

5. Gravity Gradiometry Survey System (GGSS)

The region of our interest was part of a large area surveyed for testing the gravity gradiometry survey system (GGSS) in 1987 (Jekeli, 1988). The system was built by Bell Aerospace, funded by Defense Mapping Agency, and administered by the Air Force Geophysical Laboratory for the purpose of rapid and accurate measurement of the regional gravity field. The principal motivation was to develop an accurate gravity measurement system to replace the airborne gravimtery method which was unsuccessful in the absence of mature GPS technology in those years. GGSS also suffered from poor GPS coverage during the field testing, and only 40% of the measurements were useful (Jekeli, 1993). Fortunately, some of these useful data tracks pass along the Wichita uplift (Fig. 1, the purple colored lines).

The basic idea of gravity gradiometry is to measure the curvature of the gravity field (rather than the field itself) by a pair of accelerometers located on a fixed baseline (10 cm apart for GGSS). This configuration eliminates, most importantly, the linear acceleration of the moving platform. Furthermore, other common mode noise effects are also eliminated. By rotating the baseline the

gradient signals, thus modulated at twice the rotation frequency, are separated from several errors that are modulated at once the rotation frequency. With this and various additional error-compensating technologies the system is very accurate even though the accelerometers by themselves do not possess the equivalent accuracy (Jekeli, 1988). Today, gravity gradiometry can compete with airborne gravimetry, which, however, is also robust due to the advancement of GPS technology (Jekeli, 1993). In practice, gradiometry has the further advantage that all three components of the gravity field vector can be measured independently. This is done by positioning the gradiometer baseline in different directions. For the GGSS, all five independent components of the gravity gradient tensor can be directly measured (full-tensor gradiometry). On the other hand, only the vertical gravity acceleration is typically determined in gravimetry. It has been proposed that measurements of all three components lead to better subsurface determinations compared to single component measurements (Vasco, 1989). Last, but not least, the gradiometry method responds better to the higher frequency range of the gravity spectrum so that high frequency components of the subsurface (e.g., faults) can be recovered better.

The field test of the GGSS was performed in April-May 1987. The survey was flown at 700-900 m above the ground with an aircraft speed of 400 km/hr. A total of 128 tracks were generated in a 315x315 km area. The original track spacing was 5 km. As a result of multiple elimination steps (Jekeli, 1993), a total of 19 tracks were selected to be of sufficient quality for further analysis. The tracks with the best signal quality were further tested to recover the true gravity field of the earth, by comparing to the ground gravity measurements (accurate to <1 mGal). For all three components, Brzezowski et al. (1988) reported an accuracy of 2-4 mGal based on a 90-km tie line distance (also reported by Jekeli, 1993).

The noise levels of the individual gradiometer tracks can be investigated by plotting the power spectral density (PSD) for each track. Such plots for the tracks (see, Fig. 1) are shown in Fig. 4. They show a general power-law behavior at some height from the surface (Turcotte, 1989). However, some of the tracks show erratic behavior in the gradient spectra (e.g., Tracks 27 and 39) which can be attributed to platform related effects. However, the low frequency signals are still useful in these tracks. We decided to be more conservative and eliminated Tracks 27 and 39 in our analysis. Fortunately, locations of these tracks are not of our primary geophysical interest (see, Fig. 1).

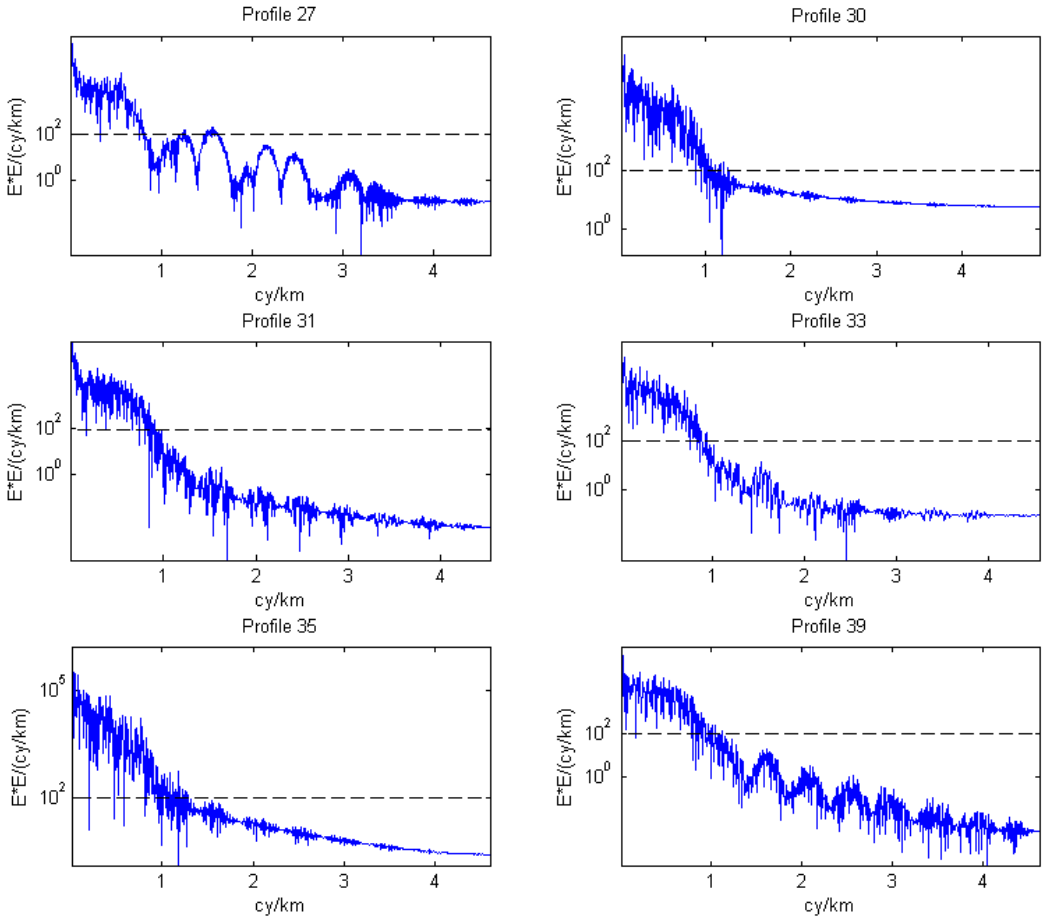

Figure 4: Power spectral densities (PSD) for the tracks in the Wichita region. Only PSDs for Tzz components are shown. Horizontal dashed lines show the average noise level reported by Brzezowski et al. (1988) based on the entire GGSS survey data.

The noise levels of the PSDs in Fig. 4 can be compared with results of other studies. Brzezowski et al. (1988) report a noise level of 800 E^2/Hz by analyzing 20 tracks in the entire survey region. For the vehicle speed of 400 km/hr, this corresponds to about 100 E^2/(cy/km) for the plots shown in Fig. 4 (the horizontal dashed lines on each panel). According to this, Tracks 31 and 33 have the best quality data with very low noise levels. Tracks 30 and 35 have somewhat higher noises but still better than the reported noise levels for the general survey. For these tracks, a rough estimate of 10 E^2/(cy/km) can be attributed to white noise for the flat part of the spectrum. For a 1-km averaging length, this corresponds to accuracy of about 3 E in the signals.

6. Qualitative Interpretations of the GGSS Data

Based on the PSD analysis four GGSS profiles (T30, T31, T33, and T35) are used for further analyses. Figs. 5-8 show the actual data for these profiles. For each figure three of the gradient components (Txx, Txz, Tzz) are shown in three panels. Because of the nearly E-W trending symmetry of the anomaly, these three components are the most interesting ones in terms of structural modeling. The other components involving E-W (y-direction) gradients are expected to show less variation in gradients. The fourth panel on each figure shows the gravity field for the corresponding profile using the EGM2008 earth gravity model (Pavlis et al., 2012) for comparison.

As reported by Brzezowski et al. (1988), a flat noise level of 1 cy/km in the frequency domain corresponds to a signal resolution of ~1 km in the space domain. Based on this, a weighted moving average with a half-window size of 2 km was applied to all profiles to remove the uncorrelated noise effects. In Figures 5-8, the origin of the x-axis corresponds to the northern boundary of the aeromagnetic data (see, Fig.1) in order to make an easier comparison of the two datasets.

Two of the GGSS tracks (T33 and T35) cross the Wichita Mountains (large red area in Fig. 1) which has a local relief of about 300 m. In this area, the gradients may include a significant effect of topography (discussed below). For the remaining profiles, terrain effects are negligibly small.

T30 (Fig. 5) is the westernmost profile (Fig. 1) cutting across the Meers fault at about x=-10 km. The changes in the gradients across the Meers fault are not significant except for Tzz (Fig. 5c). Even for the Tzz profile, large fluctuations in the data preclude to pinpoint the location of the fault visually. On the other hand, EGM2008 profile (Fig. 5d) indicates two (likely deep) density anomalies, one in the north, and one in the south. These anomalies were interpreted by Coffman et al. (1986) to be the high-density ultramafic roots of the gabbro units, and also show up as broad variations in the Tzz component of the GGSS data. On the other hand, the Txx component indicates only the southern anomaly, and lacks an indication of the northern anomaly. If the northern anomaly would have a perfectly two-dimensional symmetry along the y-direction, then the Txx and Tzz components would both carry signals with the same magnitudes and opposite signs for this anomaly. This is due to the fact that the gravity field follows Laplace's equation outside of its source, i.e., the trace of the gradient tensor must always be zero. Lack of this condition for the northern anomaly for the Txx and Tzz components suggests that the two-dimensional symmetry is violated for the anomalous body in the north at this location. On the other hand, neither of these two deep anomalies shows up in the Txz component. A distinct and sharp gradient change (> +50 E) is observed in the southern end of the Txx component. The sharp change indicates that its source is at a shallow depth. Similar types of anomalies in fact

show up in the T31 and T32 profiles. By comparing with the basement map in Fig.1, these anomalies may be attributed to the relatively high density basalt/gabbro units (Table 1) at the south end of the basement map.

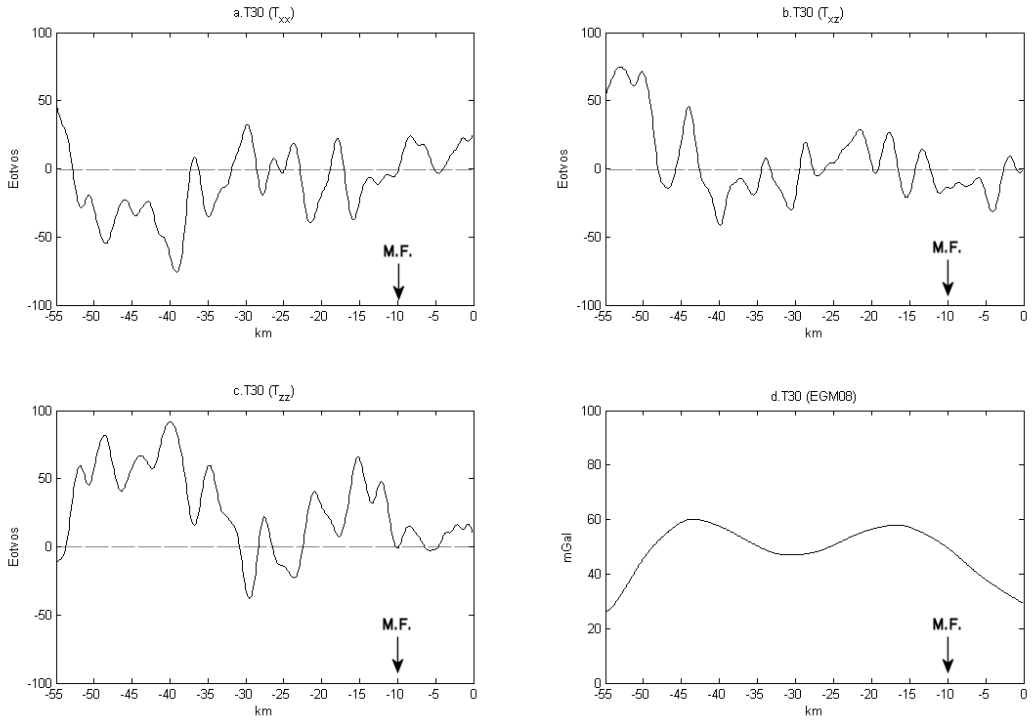

Figure 5: Profile T30; a-c) gradient profiles; d) EGM2008 gravity field.

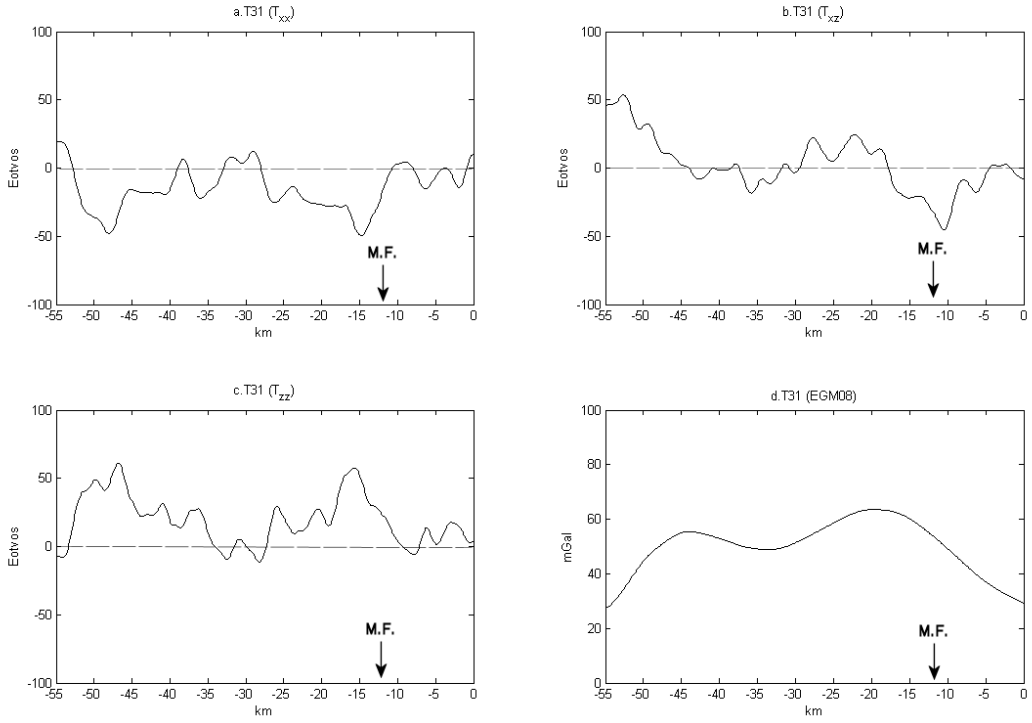

Figure 6: Profile T31; a-c) gradient profiles; d) EGM2008 gravity field.

T31 (Fig. 6) is adjacent to T30 and seems to be located on a similar structural setting (Fig. 1). The EGM2008 profile also shows a very similar pattern. Compared to T30, T31 shows less fluctuation in the gradients. Assuming no significant change in the structural regimes, the difference may be attributed the difference in the quality of the signals. As seen in Fig. 4, the noise level for T31 is significantly lower than the noise level for T30, which suggest that the local fluctuations (1-3 km wavelength) in T30 are not geophysical but instrumental. Another interesting point about T31 is that the northern anomaly shows up in both the Txx and Tzz components (unlike T30), suggesting that the northern anomaly becomes more two-dimensional here.

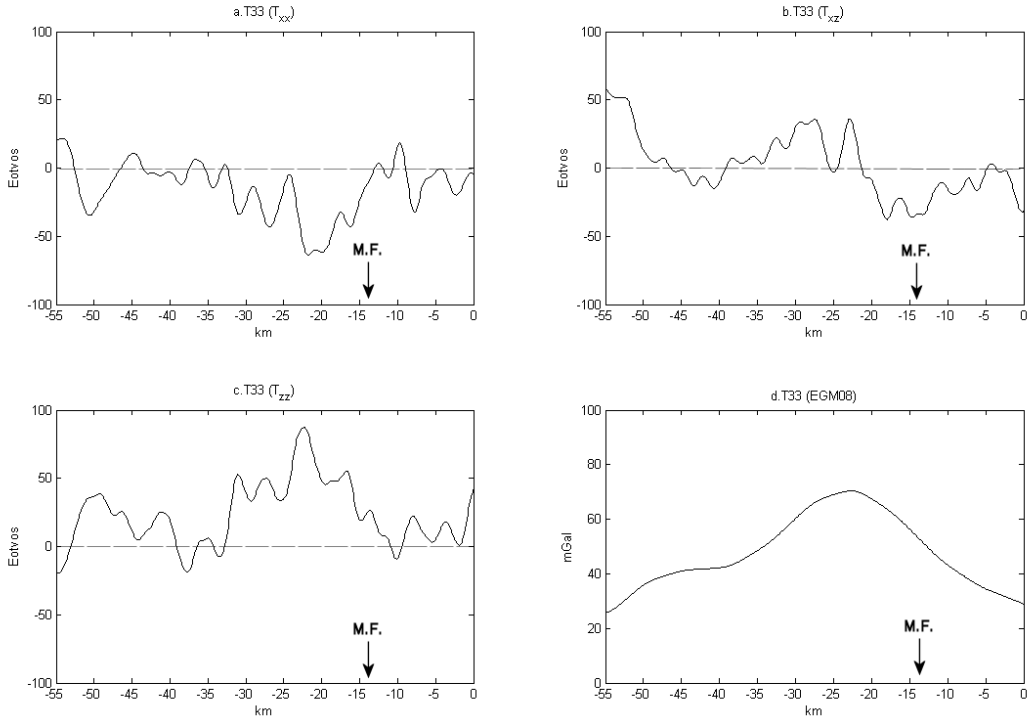

Figure 7: Profile T33; a-c) gradient profiles; d) EGM2008 gravity field.

T33 (Fig. 7) crosses almost entirely the granitic basement (Fig. 1) including the Wichita Mountains outcrop. The data show significant local fluctuations as in T30, which could also be due to instrumental effects. The EGM2008 profile shows a single broad peak in good agreement with all the gradient components. At the center of the profile where the Wichita Mountains are located, all components show anomalies, which may be attributed to the high topography.

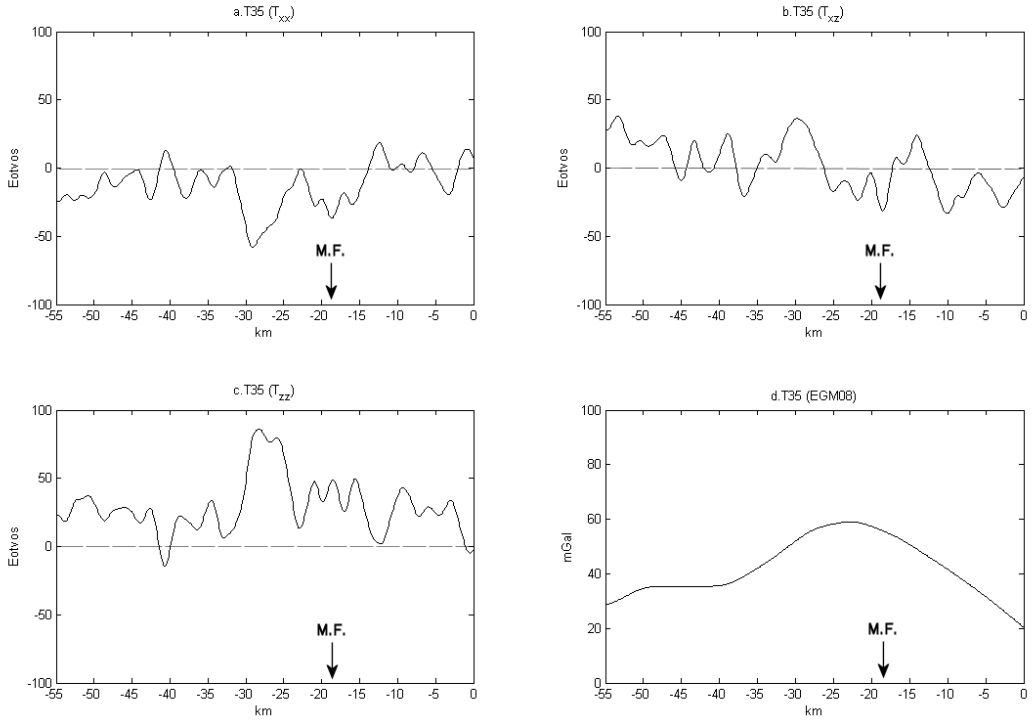

Figure 8: Profile T35; a-c) gradient profiles; d) EGM2008 gravity field.

T35 (Fig. 8) is similar to T33 in terms of both topographic and structural settings. The deep gravity anomaly becomes weaker on the EGM2008 profile here. Interestingly, none of the gradient components show this anomaly. A sharp anomaly shows up at about x=-26 km in all gradient components where the Wichita Mountains are located, which can be attributed to the topography (as opposed to EGM2008 data where no anomaly is observed).

In general, we observe that the gradient fields are sensitive to both regional and near-surface variations in the gravity field. This makes qualitative interpretation of the gradient profiles rather difficult compared to interpretations of direct gravity signals. Further quantitative analyses (e.g., various filtering operations) of the gradient profiles may be needed for interpretations of near-surface and deep sources individually. Several of these methods have been applied for the magnetic field data (Nabighian et al., 2002) and, all of these quantitative methods can be directly used for gravity gradient fields using Poisson's relation (Klingele et al., 1991; Jekeli et al., 2010).

Although gravity gradients are more sensitive to near-surface features such as fault zones, such strong anomalies were not observed in GGSS data, even though the profiles cross deeper fault zones in the region. This could be explained by the lack of density contrast between the uplifted area, and the surrounding basin sediments. As the surrounding basins are at least Permian in age,

densities of the sediments are expected to be relatively high due to compaction (densities of 2.4-2.6 g/cm^3 are reported for the basins, see, Coffman et al., 1986). This can make gravity data incapable of detecting the fault zones in this area.

7. Statistical Deconvolution of the Aeromagnetic Data

High resolution aeromagnetic data allows applications of many quantitative techniques. Most of these techniques are rooted in the statistical interpretation of the data. A number of semi-deterministic techniques were proposed for detecting fault lines and separation of anomalies in geothermal prospects in New Mexico (Grauch et al., 2001) and Nevada (Grauch et al., 2002). From a purely spectral point of view, Gregotski et al. (1991) proposed a method for deconvolution of the stochastic physical process (innovation) and obtaining better constraints for the locations of the subsurface geophysical anomalies. Agreements of the deconvolution technique with the field data clearly demonstrate the capability of the stochastic deconvolution approach, especially for detection of near-surface geologic anomalies. A similar approach was also applied in the space domain using variograms (Maus et al., 1999). Their technique also proves to be powerful for obtaining the useful high frequency components of the magnetic data. These deconvolution methods are advantageous in the sense that they return useful geologic information without applying a formal inversion to the data which suffers from the non-uniqueness. These methods are also computationally much more efficient than formal inversion techniques.

One of the unique properties of the statistical approach is the imposed well-known self-similarity (fractal behavior) of the geophysical fields. This property can be applied directly to quantitative models as a priori information (Pilkington and Todeschuck, 1990). Self-similarity is observed by studying gravity/magnetic maps at different length scales (from cm scale in well logs to thousands of kilometer scales in satellite data), which show similar patterns independent of the scale. This behavior was observed in most of the geophysical phenomena (Turcotte, 1989; Pilkington and Todoeschuck, 1990; Jensen et al., 1991).

The self-similarity is indicated by a power-law behavior in the frequency spectrum (as observed in Fig. 4). According to this, gravity or magnetic field data in 2D space at some height z can be represented by a power spectral density formula (Maus et al., 1999)

$$P(s) = cs^{-\beta+1}e^{-2zs} \qquad (1)$$

where s is the planar wave number. Here, c refers to the source intensity, and β refers to the scaling coefficient, and both have certain physical meanings. The source intensity (c) controls the magnitude of the power spectrum whereas the scaling coefficient and depth (β, z) control the

slope of the power spectral density (in log-log plots). The latter parameters have the same effect on the PSD, and they have to be traded off during modeling (Maus and Dimri, 1995). Maus et al. (1999) report the results of mapping for each of these parameters using airborne magnetic data in Africa.

Many different studies addressed the magnitude of the scaling coefficient (β) for gravity and magnetic fields. A review of these data from cm (e.g., well petrophysical logs) to km (crustal data) scales show $\beta \approx 4$ for rock magnetism (Pilkington and Todoeschuck, 1995), and $\beta \approx 3.2$ for rock mass density (Pilkington and Todoeschuck, 2004). Interestingly, the scaling coefficient (β) does not show any obvious dependence on lithology, tectonics, or any other site-specific conditions. As a result, for the most practical purposes the scaling coefficient can assumed to be constant in the modeling, while other parameters are being analyzed. This property of rock density and magnetizations indeed were used in the linear inversion applications as a priori information in the form of covariances (Tarantola and Valette, 1982; Van de Meulebrouck et al., 1984). As a result of introducing the scaling property of the sources, smoother and more realistic geophysical models were produced (Pilkington and Todoeschuck, 1990; Chasseria and Chouteau, 2003).

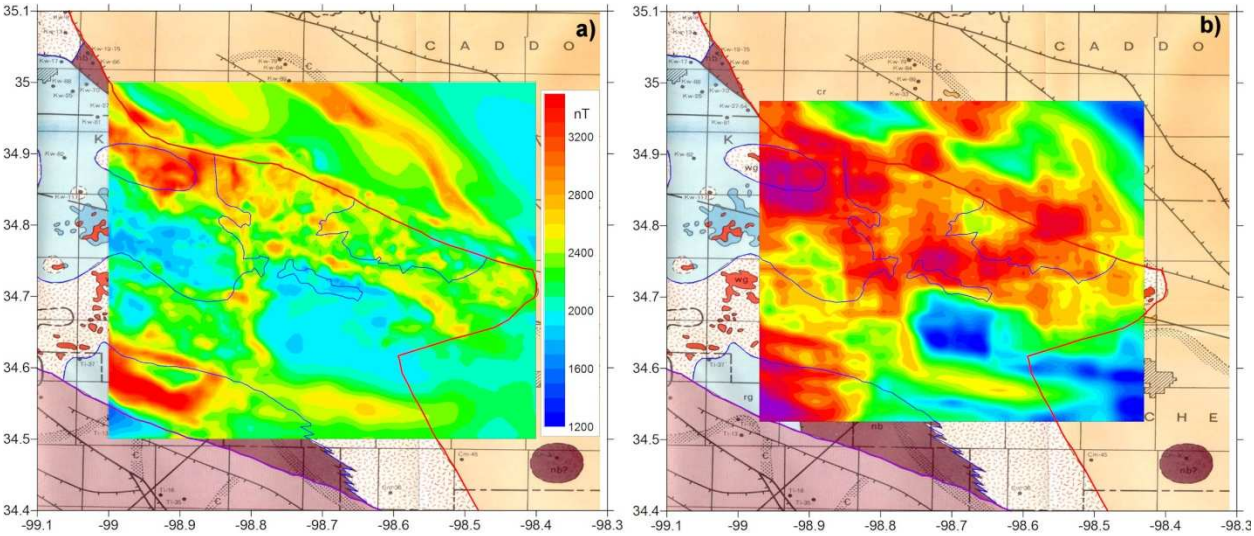

Figure 9: a) Measured (reduced-to-pole) magnetic field on the Wichita uplift region; and b) the results of the statistical deconvolution (see the text for details).

In deconvolution algorithms, a moving window is generally applied to the data and the parameters in Eq.(1) are calculated for each window. The window size depends on the wavelength interval of geophysical interest. It also depends on the survey altitude (Maus et al., 1999). In practice, assuming a statistically stationary and isotropic field, a radially averaged power spectral density (PSD) of the data can be computed for each window, and compared with the model PSD (Eq.1) to extract the geophysical parameters (e.g., Gregotski et al., 1991).

Alternatively, the model PSD can be carried to the space domain and variograms of the model and the data can be compared (e.g., Maus et al., 1999). Although this method has some advantages (such as no need for gridding), it also bears some difficulties in the treatment of variograms (Maus, 1999). As a result, we adopted the first approach, and compared the observed PSD with the model PSD for each moving window. This is a convenient approach assuming that the data have sufficiently small sampling interval for the target depths of our interest.

In the deconvolution algorithm, parameters were set to be β=3.2 and z=200 m, and the parameter c (source intensity) was extracted for each moving window. The physical size of the window was selected to be 6km x 6km (corresponding to nodal size of 11 x 11). The PSD's were compared in the interval of 0.6-0.8 1/km. As a rule of thumb, the minimum value of the frequency interval is determined by the window size whereas the maximum value is determined by the white noise in the spectrum. However, a narrower frequency band was used in modeling as a more conservative approach. The resulting source intensity map is shown in Fig. 9b, and compared with the actual (reduced-to-pole) magnetic field data in Fig. 9a.

Although the calculated source intensities shown in Fig. 9b are defined in the spectral domain they carry useful geophysical information that can be directly interpreted. As Maus and Dimri (1995) pointed out, the source intensity (c) is a function of the (vertically) averaged amplitude of the average magnetization over the considered wave number interval. The results can also be compared with apparent susceptibility maps in space-domain applications (Nabighian et al., 2002).

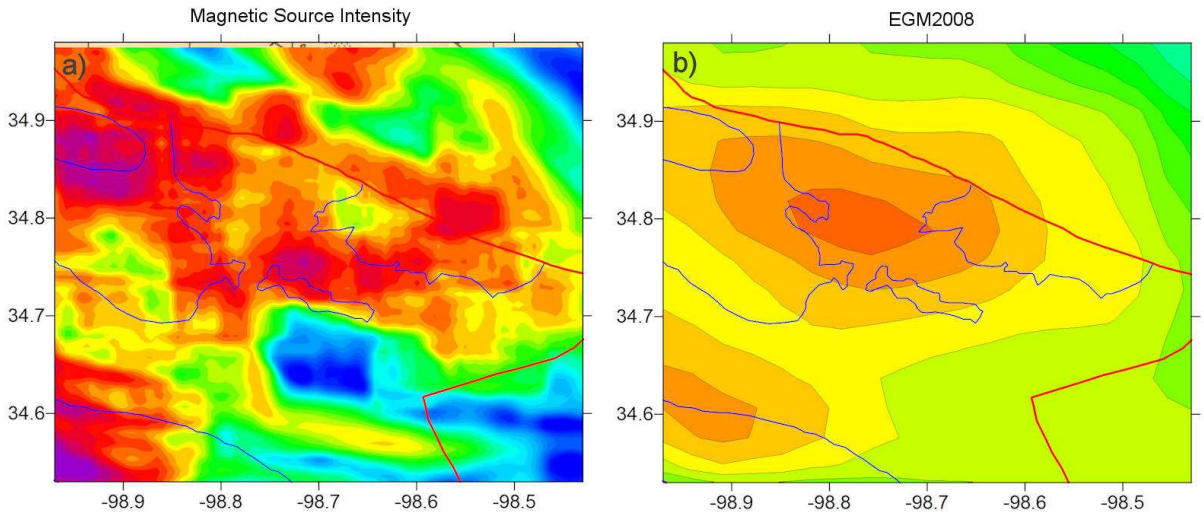

Figure 10: a) Source intensity map using statistical deconvolution of the magnetic field; b) EGM2008 gravity map of the Wichita uplift region.

The magnetic source intensity map (Fig. 9b) provides a map that is distinctly different from the magnetic field map itself (Fig 9a). For example, in the RTP magnetic field map in Fig 9a, the areas with low magnetic field values in the west disappear in the source intensity map whereas the areas with low magnetic field values in the east show up as even weaker in the source intensity map. Considering that gabbro has distinctly higher magnetization than granite (Table 1), the areas with high source intensities (orange to red colors) must delineate the areas of thick gabbroic units whereas areas with low source intensities (green to blue colors) must show areas with thick granitic bodies. The blue spot at the center of the intensity map is interesting as it correlates well with the location of the source of granitic intrusions shown by Ham et al. (1964, see, Fig. 3.) The near circular shape of the anomaly suggests that this area was the origin of silisic volcanism/magmatism.

An interesting correlation between EGM2008 and the magnetic source intensity maps is shown in Fig. 10. Two positive gravity anomalies and the high magnetic source intensities show a good spatial correlation. This suggests that both gravity and magnetic fields respond to the same structural body (i.e., the gabbro unit). A similar correlation between the gravity gradients and the magnetic field data was made before using Poisson's relation (Jekeli et al., 2010).

8. Conclusions

A qualitative geophysical analysis of the GGSS data on the Wichita uplift region shows that gradient profiles with good quality carry some useful structural information. The spectral analysis shows that certain profiles have lower instrumental noise levels, which is also supported by a comparative geophysical analysis of the gradiometry profiles. An effort for the qualitative interpretation of the gradient signals reveals that the combined high and low frequency components of the signals make visual interpretations rather difficult for gravity gradient data. Further quantitative processing of the gradient signals, such as separation of signals from shallow and deep sources, as it is conventionally done for high-resolution magnetic data, would greatly increase the effective interpretations of the gravity gradiometer data.

The statistical analysis of the aeromagnetic data on the Wichita uplift shows that spectral deconvolution of high-resolution potential field data is a powerful tool for obtaining more meaningful geophysical information. It takes advantage of the objective criteria that the field obeys the power-law behavior within a certain frequency range. The resulting source intensity maps give a more realistic view of the subsurface source distributions.

References

Brzezowski, S., D. Gleason, J. Goldstein, W. Heller, C. Jekeli, and W. White (1989), Synopsis of early field test results from the Gravity Gradiometer Survey System, Report No 482, Geodetic Science and Surveying, Ohio State University, Columbus, OH.

Chasseria, P., and M Chouteau (2003), 3D gravity inversion using a model of parameter covariance, *Journal of Applied Geophysics*, 52, 59-74.

Coffman, J.D., M.C. Gilbert, and D.A. McConnell (1986), An interpretation of the crustal structure of the southern Oklahoma aulacogen satisfying gravity data, *Oklahoma Geological Survey Guidebook*, 23, 1-10, The University of Oklahoma, Norman.

Grauch, V.J.S. (2002), High resolution aero-magnetic survey to image shallow faults, Dixie Valley geothermal field, Nevada, US Geological Survey Open-File Report 02-384.

Grauch, VJ.S., M.R. Hudson, and S.A. Minor (2001), Aeromagnetic expression of faults that offset basin fill Albuquerque basin, New Mexico, *Geophysics*, 66, 707-720.

Gregotski, M.E., O. Jensen, and J. Arkani-Hamed (1991), Fractal stochastic modeling of aeromagnetic data, *Geophysics*, 56, 1706-1715.

Ham, W.E., R.E. Denison, and C.A. Merritt (1964), Basement rocks and structural evolution of southern Oklahoma, *Oklahoma Geological Survey Bulletin*, 95, 302 pp.

Hoffman, P., J.F. Dewey, and K. Burke (1974), Aulacogens and their genetic relation to geosynclines, with a Proterozoic example from great Slave lake, Canada, in: Dott, R.H., Jr., and Shaver R.H., Modern and ancient geosynclinal sedimentation, *Society of Economic Paleontologists and Mineralogists Special Publication 19*, 38-55.

Hamilton, L.S., (1989), Structure of the Wichita uplift, Southern Oklahoma, from a wide-angle seismic experiment, M.S. Thesis, Univ. of Texas El Paso.

Jekeli, C. (1988), The gravity gradiometry Survey System (GGSS), *EOS*, 69, 105/116-117.

Jekeli, C. (1993), A review of gravity gradiometer survey system data analyses, *Geophysics*, 58, 508-514.

Jekeli, C., K. Erkan, O. Huang (2010), Gravity and pseudo-gravity: A comparison based on magnetic and gravity gradient measurements, *Proceedings of the International Symposium on Gravity, Geoid, and Earth Observations*, Chania, Crete, Grees, 23-27 June, International Association of Geodesy Symposia, 135, 123-128, Springer Verlag, Berlin.

Jensen, O.G., J.P. Todoeschuck, D.J. Crossley, and Gregotski (1991), Fractal linear models of geophysical processes, D. Schertzer and S. Lovejoy (eds), *Non-linear Variability in Geophysics*, 227-239, Kluwer Academic Publishing, The Netherlands.

Jones-Cecil, M. (1995a), Total field aeromagnetic and derivative map of the Lawton area southwestern Oklahoma: US Geological Survey Map GP-998-A, 2 sheets scale: 1:100,000, US Geological Survey.

Jones-Cecil, M. (1995b), Structural controls of Holocene reactivation of the Meers fault, southwestern Oklahoma, from magnetic studies, *Geological Society of America Bulletin*, 107, 98-112, 1995.

Keller, G.R., and W.S. Baldridge (1995), The southern Oklahoma Aulacogen, in: K.H. Olsen (Ed), Continental rifts: evolution, structure, tectonics, *Developments in Geotectonics*, 25, 427-436.

Klingele, E.E., I. Marson, and H-G. Kahle (1991), Automatic interpretation of gravity gradiometric data in two dimensions: vertical gradient, *Geophysical Prospecting*, 39, 407-434.

Lambert, D.D., D.M. Unruh, and M.C. Gilbert (1988), Rb-Sr and Sm-Nd isotopic study of the Glen Mountains layered complex: Initiation of rifting within the southern Oklahoma aulacogen, *Geology*, 16, 13-17.

Maus, S. and V. Dimri (1995), Potential field power spectrum inversion for scaling geology, *Journal of Geophysical Research*, 100, 12605-12616.

Maus, S. (1999), Variogram analysis of magnetic and gravity data, *Geophysics*, 64, 776-784.

Maus, S., K.P. Sengpiel, B. Rottger, B. Siemon, and E.A.W. Todiffe (1999), Variogram analysis of helicopter magnetic data to identify paleochannels of the Omaruru River, Namibia, *Geophysics*, 64, 785-794.

Nagibhian, M. N., V.J.S. Grauch, R.O. Hansen, T.R. LaFehr, Y. Li, J.W. Peirce, J.D. Phillips, and M. E. Ruder (2005), The historic development of the magnetic method in exploration, *Geophysics*, 70, 33ND-61ND.

Papesh, H. (1983), A regional geophysical study of the Southern Oklahoma Aulacogen, M.S. Thesis, University of Texas El Paso.

Pavlis, N.K., S.A. Holmes, S.C. Kenyon, and J.K. Factor (2012), The development and evaluation of the Earth Gravitational Model 2008 (EGM2008), *Journal of Geophysical Research*, 117, 1-38.

Price, J. D., Hogan, J. P., Gilbert, M. C., and Payne, J. D. (1998), Surface and near-surface investigation of the alteration of the Mount Scott Granite and geometry of the Sandy Creek Gabbro pluton, Hale Spring area, Wichita Mountains, Oklahoma, *Basement Tectonics* 12, 79-122.

Pruatt, M.A. (1974), The southern Oklahoma Aulacogen: A geophysical and geological investigation: M.S. Thesis, Univ. of Oklahoma, Norman, OK.

Perry, W.J., Jr (1989), Tectonic evolution of the Anadarko basin: U.S. Geological Survey Bulletin 1866-A, US Geological Survey.

Pilkington, M. and J.P. Todeschuck, (1990), Stochastic inversion for scaling geology, *Geophysical Journal International*, 102, 205-217.

Pilkington and Todoeschuck (1995), Scaling nature of crustal susceptibilities, *Geophysical Research Letters*, 22, 779-782.

Pilkington, M., and J. Todoeschuck (2004), Power-law scaling behavior of crustal density and gravity, *Geophysical Research Letters*, 31, L09606.

Robbins, S.L., and G.R. Keller (1992), Complete bouger and isostatic residual maps of the Anadarko basin, Wichita Mountains, and surrounding areas, Oklahoma, Kansas, Texas, and Colorado, *U.S. Geological Survey Bulletin 1866G*, US Geological Survey.

Tarantola, A., and B. Valette (1982), Inverse problems=quest for information, *Journal of Geophysics*, 50, 159-170.

Turcotte, D.L., (1989), Fractals in geology and geophysics, *Pure and Applied Geophysics*, 131, 171-196.

USGS (1975), Aeromagnetic map of the Wichita Mountains area, southwestern Oklahoma: U.S. Geological Survey Open-File Report 75-16, 1 sheet scale 1:62500, US Geological Survey.

Vasco, D.W. (1989), Resolution and variance operators of gravity and gravity gradiometry, *Geophysics*, 54, 889-899.

Vasco, D.W., and C. Taylor (1991), inversion of airborne gravity gradient data, southwestern Oklahoma, *Geophysics*, 56, 90-101.